Comprehensive sets of ^{124}Xe(n,γ)^{125}Xe and ^{124}Xe(n,2n)^{123}Xe cross-section data for assessment of inertial-confinement deuterium-tritium fusion plasma

Megha Bhike, B. Fallin, M. E. Gooden, N. Ludin, and W. Tornow

Phys. Rev. C **91**, 011601 — Published 7 January 2015

DOI: 10.1103/PhysRevC.91.011601

Comprehensive Sets of ^{124}Xe(n,γ)^{125}Xe and ^{124}Xe(n,2n)^{123}Xe Cross-Section Data for Assessment of Inertial Confinement Deuterium-Tritium Fusion Plasma

Megha Bhike,[1,2,*] B. Fallin,[1,2] N. Ludin,[3,†] and W. Tornow[1,2]

[1] *Department of Physics, Duke University, Durham, North Carolina, 27708, USA*
[2] *Triangle Universities Nuclear Laboratory, Durham, North Carolina, 27708, USA*
[3] *University of Denver, Denver, Colorado, 80208, USA*

(Dated: November 28, 2014)

Measurements of the neutron radiative-capture cross section of ^{124}Xe have been performed for the first time for neutron energies above 100 keV. In addition, data for the ^{124}Xe(n,2n)^{123}Xe reaction cross section have been obtained from threshold to 14.8 MeV to cover the entire energy range of interest, while previous data existed only at around 14 MeV. The results of these measurements provide the basis for an alternative and sensitive diagnostic tool for investigating properties of the inertial confinement fusion plasma in Deuterium-Tritium (DT) capsules at the National Ignition Facility located at Lawrence Livermore National Laboratory. Here, areal density ρR (density $\times$ Radius) of the fuel, burn asymmetry and fuel-ablator mix are of special interest. The ^{124}Xe(n,γ)^{125}Xe reaction probes the down-scattered neutrons, while the ^{124}Xe(n,2n)^{123}Xe reaction provides a measure of the 14 MeV direct neutrons.

PACS numbers: 52.57.-z,24.10.Pa,29.30.Kv,25.40.Lw

Nuclear reactions play an important role in understanding the complicated physics governing the Inertial Confinement Fusion (ICF) plasma [1, 2]. The neutron energy distribution created in Deuterium-Tritium (DT) ICF plasmas depends, among other parameters, to some extent on the stopping power of deuterons and tritons in the plasma. This is especially the case for the reaction-in-flight neutrons with energies between 15 and 30 MeV [3]. A diagram of a special DT capsule is shown in Fig. 1. The radius of the capsule is 1.1 mm. The outer ablator consists of plastic or beryllium, which almost completely burns away when hit by the lasers. About 10^{15} atoms of the isotope(s) of interest will be loaded into the inner-most layer of the ablator shell [4, 5], which in turn surrounds a layer of DT ice and a sphere of DT gas. Noble gases are considered to be the most suitable dopants. For many reasons, ^{124}Xe became the primary choice of capsule dopant [4]. In the presence of DT neutrons the isotope ^{124}Xe undergoes both (n,γ) and (n,2n) reactions, leading to ^{125}Xe and ^{123}Xe, respectively. Following a NIF shot, the xenon gas is collected with the Radiochemical Analysis of Gaseous Samples (RAGS) [5], and subsequently, the two isotopes ^{125}Xe and ^{123}Xe are analyzed using gamma-ray spectroscopy to determine the ^{125}Xe/^{123}Xe ratio. The collection efficiency cancels, and there is no need to know the absolute amount of ^{124}Xe bonded to the ablator. Therefore, the capsule performance can be benchmarked according to the ^{125}Xe/^{123}Xe ratio.

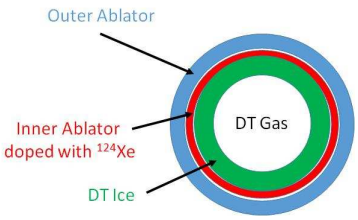

FIG. 1: (Color online)Schematic of Deuterium-Tritium capsule used in laser shots at the National Ignition Facility.

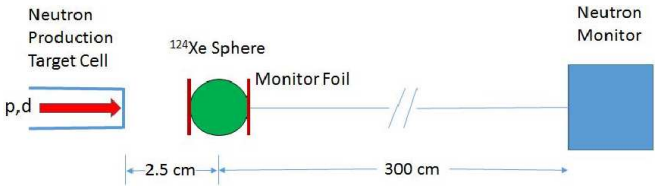

FIG. 2: (Color online)Schematic of experimental setup consisting of neutron production target, ^{124}Xe high-pressure sphere with monitor foils, and neutron flux detector.

The threshold for the ^{124}Xe(n,2n)^{123}Xe reaction is 10.569 MeV, and its cross section increases with energy in the neutron energy region of interest. Therefore, this reaction probes the primary 14 MeV DT neutrons and a small portion of the down-scattered neutrons (small-angle scattering). In contrast, the energy threshold of the ^{124}Xe(n,γ)^{125}Xe reaction is zero, and its cross section increases with decreasing neutron energy. With increasing areal density ρR of the fuel, more neutrons will down-scatter to lower energies, thereby increasing the ^{125}Xe activity at the expense of the ^{123}Xe activity. Therefore, the ^{125}Xe/^{123}Xe intensity ratio provides a measure for ρR of the ICF plasma [4].

A NIF shot on a spherical glass shell of 1.1 mm radius filled with a 1:1 DT mixture and a small amount of ^{124}Xe was performed already as early as 2011 for commissioning

*Electronic address: megha@tunl.duke.edu
†NSF REU 2013 student at TUNL

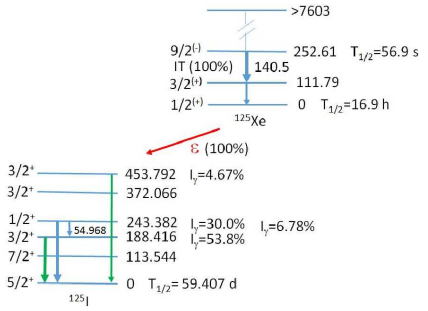

FIG. 3: (Color online)Partial level scheme relevant to the ^{124}Xe(n,γ)^{125}Xe reaction. All energies are given in keV. Data taken from [16].

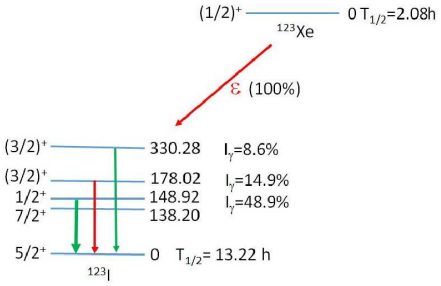

FIG. 4: (Color online)Partial level scheme relevant to the ^{124}Xe(n,2n)^{123}Xe reaction. All energies are given in keV. Data taken from [16].

of the RAGS [5, 6]. The data of a more recent shot are being analyzed [7]. However, cryogenically layered capsules (see Fig. 1) loaded with xenon have not been used yet at NIF [7]. Currently, any quantitative assessment of the areal density ρR of the DT plasma obtained from ^{124}Xe loaded capsules rests on the accuracy of evaluations and model calculations used for the ^{124}Xe(n,γ)^{125}Xe and ^{124}Xe(n,2n)^{123}Xe reaction cross sections. One reason for choosing ^{124}Xe as a dopant is its evaluated [8] and predicted extremely large (n,γ) cross section. For example, at 3 MeV neutron energy this cross section is predicted to be a factor of 300 larger than that for the neutron rich isotope ^{136}Xe [8, 9]. However, for the neutron-deficient isotope ^{124}Xe no experimental data exist for the (n,γ) reaction above 30 keV neutron energy [8]. Furthermore, for the (n,2n) cross section experimental data exist only at around 14 MeV [10–12] and they scatter between 1.0 and 1.6 b. Therefore, to improve the accuracy of ρR determinations from ^{125}Xe/^{123}Xe ratio measurements at NIF, cross-section data for the ^{124}Xe(n,γ)^{125}Xe reaction were measured in the important energy range between 0.4 and 7.5 MeV. In addition, cross-section data for the ^{124}Xe(n,2n)^{123}Xe data were obtained between 11.3 and 14.8 MeV. The experimental procedure and our results are presented in the following.

Monoenergetic neutrons were obtained via the ^{3}H(p,n)^{3}He reaction (Q=-0.764 MeV) between 0.37 and 3.8 MeV, via the ^{2}H(d,n)^{3}He reaction (Q=+3.269 MeV) between 4.5 and 14.5 MeV, and finally at 14.8 MeV via the ^{3}H(d,n)^{4}He reaction (Q=+17.589 MeV). The charged-particle beams were produced and accelerated at the Triangle Universities Nuclear Laboratory (TUNL) [13]. Typically, the proton and deuteron beam currents ranged between 1.5 μA and 3.5 μA, producing the neutron fluxes given in Table I and Table III in the second column at the neutron energies specified in the first column. The target assemblies used for the ^{3}H(p,n)^{3}He, ^{3}H(d,n)^{4}He and ^{2}H(d,n)^{3}He reactions were identical to those of Ref. [9] and Ref. [14], respectively.

A schematic view of the experimental setup is shown in Fig. 2. The xenon gas, enriched to 99.6% in ^{124}Xe, was contained in a stainless steel sphere with inner diameter of 20 mm and wall thickness of 0.6 mm, resulting in a ^{124}Xe mass of 2.697 g and a pressure of about 120 atm. The distance between the end of the neutron production target and the center of the ^{124}Xe sphere was typically 19 mm for measurements of the ^{124}Xe(n,γ)^{125}Xe reaction cross section, and 25 mm for the ^{124}Xe(n,2n)^{123}Xe reaction. Monitor foils (indium and gold) were attached to the upstream and downstream faces of the sphere for neutron fluence determination. The entire neutron target-sphere assembly was contained in a thin-walled cage made of 0.5 mm thick cadmium to prevent room-return thermal neutrons from initiating the ^{124}Xe(n,γ)^{125}Xe reaction. The room-return neutron flux is five to six orders of magnitude smaller than the direct neutron flux of interest [15].

A neutron flux monitor was positioned at 0° relative to the incident charged-particle beam at a distance of 3 m from the neutron-production target. This BC-501A based liquid scintillator [17] of 3.9 cm diameter and 3.9 cm thickness was used to record the neutron flux during the activation measurements.

The tritiated titanium target [14] used for producing neutrons via the ^{3}H(p,n)^{3}He reaction is also the source of lower energy background neutrons, once the proton energy exceeds about 3 MeV. Therefore, as described in Ref. [9], for neutron energies between 2.4 and 3.8 MeV, auxiliary measurements were performed with an untritiated, but otherwise identical target, to correct the data of interest for contributions originating from (p,n) reactions in the titanium layer and copper backing of the tritiated titanium target assembly. The correction factors were between 1.7% at 2.73 MeV and 28% at 3.61 MeV. Similarly, for the ^{2}H(d,n)^{3}He reaction at E_n = 6.31 MeV and 7.25 MeV gas-out measurements were made to correct for the deuteron breakup reaction on the structural materials of the deuterium gas cell. The size of the corrections varied between 1% at 5.31 MeV and 40% at 7.31 MeV for the reaction ^{124}Xe(n,γ)^{125}Xe. The correction factors associated with the monitor foils varied between 0.1% at 5.31 MeV and 7% at 3.61 MeV.

For the measurements of the ^{124}Xe(n,γ)^{125}Xe cross section the neutron irradiation times varied between 1.5 h and 4 h (depending on energy), while for the ^{124}Xe(n,2n)^{123}Xe reaction activation times between 1 h

and 1.5 h turned out to be sufficient. After irradiation, the ^{124}Xe sphere was γ-ray counted using a calibrated and shielded 60% High-Purity Germanium (HPGe) detector of well-known efficiency. For the ^{124}Xe(n,γ)^{125}Xe reaction, the γ-ray lines of 188.416 and 243.382 keV from ^{125}I were used after allowing for a delay time of 10 minutes for the 252.61 keV isomeric state of ^{125}Xe to decay to its ground state (see Fig. 3). For the ^{124}Xe(n,2n)^{123}Xe cross-section measurements the yields of the ^{123}I γ-ray lines at 148.92 and 178.02 keV were recorded (see Fig. 4). The indium and gold foils were γ-ray counted using 60% HPGe detectors as well. The data-acquisition system GENIE [18] was used to follow the intensity of the γ-ray lines of interest over typically three half-life times, except for the 355.73 keV line of ^{196}Au ($T_{1/2}$=6.167 d), for which data-acquisition was limited to 24 hours. The γ-ray spectra were analyzed with the software package TV [19].

An empty, but otherwise identical sphere was irradiated at selected energies to check whether γ-ray lines from the stainless steel sphere were contaminating the lines of interest. No such γ-ray lines were observed. The well-known activation formula [9] was used to determine the neutron flux ϕ_n at the position of the ^{124}Xe sphere from the data obtained with the monitor foils.

$$A = N\sigma\phi_n\epsilon I_\gamma(1-e^{-\lambda t_i})e^{-\lambda t_d}(1-e^{-\lambda t_m}). \quad (1)$$

Here, the activity A is the total yield in the photopeak of the monitor reaction, N is the number of target nuclei, σ is the reaction cross section, ϵ is the photopeak efficiency at the γ-ray energy of interest, I_γ is the branching ratio, and λ denotes the decay constant of the residual nucleus. The times t_i, t_d, and t_m refer to the irradiation time, decay time between the end of irradiation and beginning of counting, and the measuring time, respectively. The ^{115}In(n,n$'$)^{115m}In reaction was used for incident neutron energies between 0.85 and 7.31 MeV. Cross-section values were obtained from Ref. [20]. The ^{197}Au(n,γ)^{198}Au reaction was used at 0.37 MeV, with the cross section taken from Ref. [21]. Finally, the reaction ^{196}Au(n,2n)^{196}Au was employed at energies above 9 MeV. In this case the cross-section values of Ref. [22] were used. Details are given in the third column of Table III.

Subsequently, the activation formula was employed again. This time with the neutron flux ϕ_n determined above to extract the cross sections σ of interest, now using the relevant quantities related to ^{124}Xe.

The tight geometry of the experimental setup shown schematically in Fig. 2, and the neutron attenuation in the ^{124}Xe sphere causes the neutron fluence at the position of the ^{124}Xe gas to deviate from the average fluence obtained from the two monitor foils. In addition, the average neutron energy seen by the ^{124}Xe gas is not the nominal neutron energy measured with the neutron monitor positioned at 0°, or calculated from the reaction kinematics at 0°. A Monte-Carlo code was written to obtain the effective neutron fluence, average neutron energy and its associated energy spread seen by the ^{124}Xe gas. Because of the shorter distance between the neutron production target and the ^{124}Xe sphere, the fluence correction factors were up to 12% for the data obtained with the ^{3}H(p,n)^{3}He and ^{3}H(d,n)^{4}He reactions, but did not exceed 2% for the ^{2}H(d,n)^{3}He reaction.

The activity of the ^{124}Xe gas was measured with the center of the stainless steel sphere positioned at a distance of 50 mm from the front face of the 68 mm diameter HPGe detector. The absolute efficiency of the HPGe detector was measured with standard test sources, including a multi γ-ray source (consisting of ^{54}Mn, ^{57}Co, ^{65}Zn, ^{88}Y, ^{109}Cd, ^{113}Sn, ^{134}Cs, ^{137}Cs, ^{139}Ce, ^{203}Hg and ^{241}Am), also positioned at a distance of 50 mm. However, because of the geometry difference between these test sources (a few mm diameter and very thin) and the ^{124}Xe gas (20 mm diameter) and the monitor foils, Monte-Carlo calculations were performed to correct for this geometry effect, as well as for the self-absorption of the γ-ray lines of interest in the gas and the stainless steel wall of the sphere. Depending on γ-ray test source diameter and γ-ray energy (from ^{125}I and ^{123}I), the total corrections varied between 15 and 47%. The correction

TABLE I: ^{124}Xe(n,γ)^{125}Xe reaction: Neutron energy and associated energy spread, Neutron flux at position of ^{124}Xe sphere, monitor reactions used for determining the neutron fluence, and cross-section results obtained for ^{124}Xe(n,γ)^{125}Xe reaction.

Neutron Energy $E_n \pm \triangle E_n$ (MeV)	Neutron Flux ϕ_n (cm^{-2}s^{-1})	Monitor Reactions σ (mb)	^{124}Xe(n,γ)^{125}Xe σ (mb)
0.37±0.10	1.04×10^7	183.90±8.90	266.92±15.44
0.86±0.10	4.09×10^6	166.44±1.70	176.14±11.20
1.86±0.10	1.06×10^7	229.72±5.50	141.96±9.92
2.73±0.15	9.49×10^6	344.50±8.10	126.14±20.31
3.61±0.15	5.72×10^6	331.51±7.80	133.62±24.22
4.48±0.26	7.21×10^6	318.44±7.48	64.14±5.61
5.31±0.35	2.29×10^7	334.57±8.70	29.51±5.32
6.31±0.33	2.60×10^7	346.09±12.30	22.78±3.46
7.25 ±0.33	4.28×10^7	323.22±11.50	16.10±2.93

TABLE II: Uncertainty budget for ^{124}Xe(n,γ)^{125}Xe and monitor reaction cross-section data.

Uncertainty	^{124}Xe (%)	Monitors (%)
Counting statistics	0.1-1.16	0.3-1.13
Reference cross sections	-	2.3-4.1
Neutron flux correction	< 2	-
Detector efficiency	0.91-5.30	1.16-3.14
Source geometry and self-absorption	<0.2	<0.2
Half-life time	1.18	0.09-0.31
γ-ray branching ratio I_γ	-	1.42-4.80
Neutron flux fluctuation	<1	<1
Low-energy neutrons	<4	<1

TABLE III: ^{124}Xe(n,2n)^{123}Xe reaction: Neutron energy and associated energy spread, Neutron flux at position of ^{124}Xe sphere, monitor reactions used for determining the neutron fluence, and cross-section results obtained for ^{124}Xe(n,2n)^{123}Xe reaction.

Neutron Energy $E_n \pm \triangle E_n$ (MeV)	Neutron Flux ϕ_n ($cm^{-2}s^{-1}$)	Monitor Reactions σ (mb)	^{124}Xe(n,2n)^{123}Xe σ (mb)
11.36±0.14	1.57×10^7	1564.05±42.07	80.36±5.03
11.86±0.14	2.32×10^7	1701.31±44.06	228.56±12.17
12.36±0.14	2.07×10^7	1823.51±44.68	391.22±34.25
12.85±0.15	1.82×10^7	1933.86±43.90	570.07±28.46
13.35±0.15	1.84×10^7	2035.41±37.86	676.28±39.99
13.85±0.15	2.03×10^7	2114.60±26.43	793.88±38.13
14.35±0.15	1.82×10^7	2152.99±24.09	839.57±46.53
14.80±0.07	6.14×10^6	2164.20±22.83	909.44±46.87

TABLE IV: Uncertainty budget for ^{124}Xe(n,2n)^{123}Xe and monitor reaction cross-section data.

Uncertainty	^{124}Xe (%)	Monitors (%)
Counting statistics	0.1-0.2	0.35-0.62
Reference cross sections	-	1-2.7
Neutron flux correction	< 2	-
Detector efficiency	1-4	4-5
Source geometry and self-absorption	<0.2	<0.2
Half-life time	0.96	0.01
γ-ray branching ratio I_γ	-	-

factors for the monitor foils varied between 1 and 2%.

The results for the ^{124}Xe(n,γ)^{125}Xe cross section are given in the 4^{th} column of Table I. The quoted uncertainty reflects the total uncertainty obtained by adding the individual uncertainties specified in Table II in quadrature. The present results are shown in Fig. 5 in comparison to predictions based on the evaluations ENDF-B/VII.1 [8] and JENDL-4.0 [23] and the model calculation TENDL-2012 and TENDL-2013 of the TALYS nuclear reaction code [24]. As can be seen, none of the predictions is in good agreement with the experimental data. The magnitude of the ^{124}Xe(n,γ)^{125}Xe cross section is described best by the most recent TALYS calculation.

The results for the ^{124}Xe(n,2n)^{123}Xe cross section are given in the 4^{th} column of Table III. The uncertainty budget is summarized in Table IV. The present results are compared in Fig. 6 to the two evaluations and the model calculation referred to above, and the previous data at around 14 MeV. The present data follow the predicted energy dependence, and are only slightly lower in magnitude than the ENDF-B/VII.1 [8] evaluation. In the 14 MeV region our data are slightly below the datum of Sigg et al. [11] and Kondaiah et al. [10], while the data of Bazan [12] are inconsistent with both the new data and the two previous data sets.

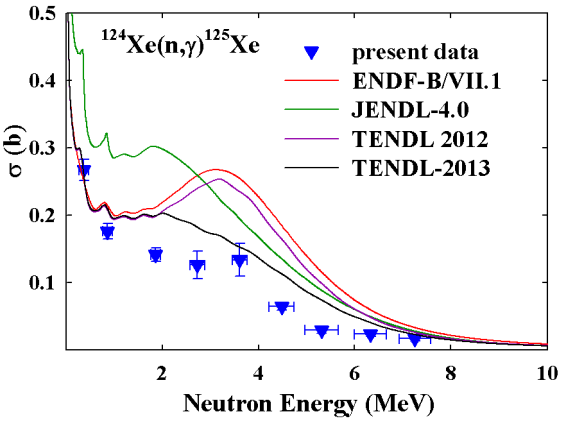

FIG. 5: (Color online)^{124}Xe(n,γ)^{125}Xe cross-section data obtained in the present work in comparison to the evaluations ENDF-B/VII.1 [8] and JENDL-4.0 [23], and the model calculation TENDL-2012 [24].

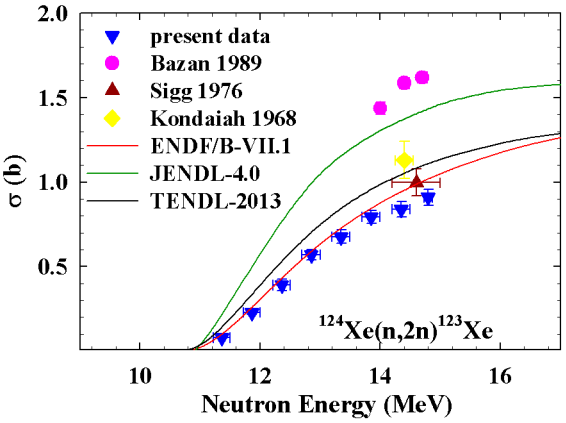

FIG. 6: (Color online)^{124}Xe(n,2n)^{123}Xe cross-section data in comparison to evaluations [8, 23, 24] and previous data [10–12]. The calculations of TENDL-2012 and TENDL-2013 are identical.

In summary, the ^{124}Xe(n,γ)^{125}Xe and ^{124}Xe(n,2n)^{123}Xe cross-section data obtained in the present work provide for the first time an accurate basis for interpreting measurements of the ^{125}Xe/^{123}Xe intensity ratio performed at NIF in laser shots on ^{124}Xe loaded DT capsules. It is anticipated that the extracted information will add to the understanding of the exciting physics governing the inertial confinement fusion plasma.

We thank Ronald Schwengner, Technical University Dresden, Germany, for providing the ^{124}Xe filled and empty spheres. The authors acknowledge valuable contributions from A. P. Tonchev, LLNL, M. Boswell, LANL, S. W. Finch, Duke University, and M. E. Gooden, North Carolina State University. This work was supported in part by the National Nuclear Security Administration under the Stewardship Science Academic Alliance Pro-

gram through the US Department of Energy Grant No. DE-NA0001839, and by the US Department of Energy, Office of Nuclear Physics, under Grant No. DE-FG02-97ER41033.

[1] J. A. Frenje *et al.*, Nucl. Fusion **53**, 043014 (2013).
[2] P. A. Bradley, G. P. Grim, A. C. Hayes, G. Jungman, R. S. Rundberg, J. B. Wilhelmy, G. M. Hale, and R. C. Korzekwa, Phys. Rev. C **86**, 014617 (2012).
[3] J. Lindl *et al.*, Phys. Plasmas **21**, 020501 (2014).
[4] D. A. Shaughnessy, C. Cerjan, K. J. Moody, L. Bernstein, R. Hoffman, M. A. Stoyer, R. Fortner, and D. Schneider, Lawrence Livermore National Laboratory Report No. LLNL-TR-472995 (2011).
[5] D. A. Shaughnessy, C. A. Velsko, D. R. Jedlovec, C. B. Yeamans, K. J. Moody, E. Tereshatov, W. Stoeffl, and A. Riddle, Rev. Sci. Instrum. **83**, 10D917 (2012).
[6] https://str.llnl.gov/Dec12/shaughnessy.html
[7] D. A. Shaughnessy, private communication, 2014.
[8] M. B. Chadwick *et al.*, Nucl. Data Sheets **112**, 2887 (2011).
[9] M. Bhike, and W. Tornow, Phys. Rev. C **89**, 031602(R) (2014).
[10] E. Kondaiah, N. Ranakumar, and R. W. Fink, Nucl. Phys. A **120**, 337 (1968).
[11] R. A. Sigg, and P. K. Kuroda, Nucl. Sci. and Eng. **60**, 235 (1976).
[12] F. Bazan, LLNL Internal Report UCRL-53929, 162 (1989).
[13] http://www.tunl.duke.edu/
[14] M. Bhike, B. Fallin, and W. Tornow, Phys. Lett. B **736**, 361 (2014)
[15] C. Bhatia *et al.*, Nucl. Instr. and Meth. in Phy. Res. A **757**, 7 (2014).
[16] http://www.nndc.bnl.gov
[17] http://www.detectors.saint-gobain.com
[18] http://www.canberra.com
[19] J. Theuerkauf, S. Esser, S. Krink, M. Luig, N. Nicolay, O. Stauch, and H. Wolters, Program TV, Institute for Nuclear Physics, University of Cologne (1993) (unpublished).
[20] A. B. Smith, S. Chiba, D. L. Smith, J. W. Meadows, P. T. Guenther, R. D. Lawson, and R. J. Howerton, ANL/NDM-115 (1990).
[21] A. N. Davletshin, E. V. Teplov, A. O. Tipunkov, S. V. Tikhonov, and V. A. Tolstikov, Vop. At. NaukiiTekhn., Ser. Yadernye Konstanty **1**, 13 (1993).
[22] K. I. Zolotarev *et. al.*, INDC(NDS)-526 (2008).
[23] K. Shibata *et al.*, Nucl. Sci. Technol. **48**, 1 (2011).
[24] A. J. Koning, S. Hilaire, and M. C. Duijvestijin, AIP Conf. Proc. No. 769, 1154 (2005).